Supporting Information

NaNbO₃/MoS₂ and NaNbO₃/BiVO₄ Core/Shell Nanostructures for Photoelectrochemical Hydrogen Generation

Sandeep Kumar,[†] Tamanna Malik,[†] Deepanshu Sharma,[‡] and Ashok K. Ganguli[†]*

[†]Department of Chemistry, Indian Institute of Technology, HauzKhas, New Delhi 110016, India

[‡]Department of Physics, Indian Institute of Technology, HauzKhas, New Delhi 110016, India

* Author for correspondence
e-mail: ashok@chemistry.iitd.ernet.in
Tel No. 91-11-26591511
Fax   91-11-26854715

Characterization:

Powder X-Ray Diffraction (PXRD)

Each crystalline phase has a characteristic powder XRD pattern which can be used as a fingerprint for identification purposes and for obtaining details regarding the phase purity, crystallinity and crystallite size of the as-synthesized samples. For this purpose we used Bruker D8 Advance diffractometer machine equipped with Ni-filtered Cu K_α radiation (λ = 1.5418Å) in the 2θ range of 10−70° at a scanning rate of 0.02° per second.

The strain developed during the shell formation in core-shell heterostructures was estimated by Williamson-Hall plot using the following equation[1]

$$\beta\cos\theta/\lambda = 1/D + \eta\sin\theta/\lambda \qquad (1)$$

Where β is the full width at half-maximum (fwhm) of the θ−2θ peak, θ is the diffraction angle, λ is the X-ray wavelength, η is the effective strain, and D is the crystallite size. The strain (η) is calculated from the slope and the crystallite size (D) is calculated from the intercept of a plot of $\beta\cos\theta/\lambda$ against $\sin\theta/\lambda$.

The crystallite sizes obtained using Williamson-Hall plot were corroborated with the crystallite sizes (D_{Sch}, in Å) calculated by the application of the Scherrer's formula (equation 2) to the PXRD data:[2]

$$D_{Sch} = K\lambda/\beta\cos\theta \qquad (2)$$

Where λ is the wavelength of Cu Kα radiation, β is the corrected half width of the

diffracted peak, θ is the diffraction angle, and K is equal to 0.9.

Field-Emission Scanning Electron Microscopy (FESEM)

Field-emission scanning electron microscopy (FEI QUANTA 3D FEG) was used for determination of the surface morphologies and elemental composition confirmation of all the synthesized materials. For sample preparation, a small amount of dry and finely grounded powdered sample was spread on carbon tape adhered to an aluminum stub and sputter-coated by an ultrathin layer of gold prior to the studies to prevent sample charging effects. The measurement was carried out on an FESEM at accelerating voltage of 5 kV equipped with an energy dispersive X-ray spectroscopy (EDS) detector for elemental mapping.

Transmission electron microscopy (TEM)

TEM and high-resolution transmission electron microscopy (HRTEM) studies were used to achieve exhaustive insights into the morphology of the resultant core-shell heterostructures. Samples prepared for TEM analysis via dispersing the samples in ethanol with the help of ultrasonication and subsequently droplets of the suspension onto a carbon-coated Cu grid. Images were captured on JEOL 200 KV TEM, with a high brightness field-emission gun (FEG) source which produces improved sensitivity and resolution compared to more traditional thermionic sources like LaB6 or Tungsten filaments. Collected TEM and HRTEM images of synthesized nanomaterials provide detailed information about the size, shape and morphology of materials.

UV−Vis Diffuse Reflectance Spectra (UV−Vis DRS)

The optical properties of as-synthesized samples in the pressed disk form were analyzed by UV−Vis diffuse reflectance spectroscopy recorded on a Shimadzu UV-2450 spectrometer equipped with an integrating sphere assembly, over a wavelength range of 250−800 nm employing $BaSO_4$ as a reflectance standard. The Tauc plot is a method widely used for the determination of band gap. The process for obtaining band gap using Tauc plot is as follows:

The following expression (equation 3) proposed by Tauc, Davis, and Mott[3] is used:

$$(\alpha h\nu)^{1/n} = A (h\nu - E_g) \qquad (3)$$

Where h is Planck's constant, ν is frequency of vibration, α: absorption coefficient, E_g is band gap and A is proportionality constant. The value of the exponent n denotes the nature of the transition. For direct allowed transition (n = 1/2), for direct forbidden transition (n = 3/2), for indirect allowed transition (n = 2) and for indirect forbidden transition: n = 3. Since the direct allowed transition is possible in the synthesized materials hence n = 1/2 was used as the exponent in equation (3).

The acquired diffuse reflectance spectrum was converted to Kubelka-Munk function. Thus, the vertical axis is converted to quantity $F(R_\infty)$, which is proportional to the absorption coefficient. The α in the Tauc equation is substituted with $F(R_\infty)$ and the expression becomes:

$$(h\nu F(R_\infty))^2 = A(h\nu - E_g) \qquad (4)$$

Kubelka-Munk function was used and $(h\nu F(R_\infty))^2$ was plotted against $h\nu$ and the intercept drawn against X-axis for calculation the band gap values.

Photoelectrochemical Studies

For photoelectrochemical (PEC) water-splitting measurements, we prepared electrodes of synthesized bare materials and the core-shell heterostrucrures. The current–voltage (I-V), Mott-Schottky and electrochemical impedance spectroscopy analysis was carried out by using the PEC cells with fabricated photoelectrode. 0.5M Na_2SO_4 solution was used as electrolyte and measurements were recorded in the dark and under illumination with a 150 W Xe arc lamp.[4] The photoresponse was observed through the current–voltage and EIS measurements and noticeable change was observed under illumination clearly revealing the photoactivity of the designed heterostructures.

Photocatalytic Activity

Photocatalytic activities of the synthesized core-shell heterostructures were analyzed by observing their abilities to degrade the Rhodamine B (RhB) dye under visible light irradiation. The experiment was conducted in aqueous solution under simulated visible light irradiation using a 300 W xenon arc lamp equipped with UV cut off filter to remove the radiation below 420 nm. The measurement tests were performed in a reactor equipped with a cooling water system to keep the temperature constant. In a typical visible-light photocatalytic experiment, initially the catalyst (40 mg) was dispersed in a 100 mL aqueous solution of RhB (1×10^{-5} M) and the obtained catalyst suspensions were magnetically stirred at 450 rpm in the dark for 45 minutes to ensure proper adsorption/desorption equilibrium between catalyst and organic dye. The catalyst suspension was subsequently irradiated with visible light to initiate the photocatalytic reaction. Adequate aliquots (1.5 mL) of the suspension were extracted

and centrifuged at 8,000 rpm after every 5-10 min during the course of 80 minutes (under irradiation) to remove the residual catalyst particulates for analysis. Analogous control experiments were performed either without catalyst or in the dark to attest that the degradation reaction is solely driven by a photocatalytic process. The photo degradation efficiency was monitored by measuring the change in intensity of the characteristic absorbance of RhB at 554 nm (taken in quartz cells with 10 mm path length) using Shimadzu UV 2450 spectrometer. The photo catalytic ability or degradation efficiency (DE) of the resultant samples was calculated from the following relation:

$$DE\ (\%) = (C_0 - C)/C_0 \times 100 \qquad (5)$$

Where C_0 refers to the absorbance of RhB after the adsorption equilibrium is achieved prior to the visible light illumination, and C refers to the absorbance of the RhB at time interval 't' under visible light illumination.

Photoluminescence (PL) and Time resolved studies

For study of the charge recombination, substitute of photogenerated charge carriers at the interface (which govern the efficiency of the photocatalyst) we have performed photoluminescence (PL) and time resolved spectroscopy measurements. The photoluminescence (PL) spectra of the as-synthesized samples in form of disks were investigated at room temperature on a Fluoromax-4 fluorescence spectrophotometer (Horiba Jobin Yvon Japan) with an excitation wavelength (λex) of 340 nm with the excitation and emission slit width of 2 and 5 nm, respectively.

Table S1: d-spacing values of NaNbO$_3$ and core-shell heterostructures after composite formation see below.

S. No.	Peaks 2θ	NaNbO$_3$ d-Values (Å)	Peaks 2θ	NaNbO$_3$/MoS$_2$ d-Values (Å)	Peaks 2θ	NaNbO$_3$/BiVO 4 d-Values (Å)
1.	22.62°	3.923	22.65°	3.913	22.69°	3.911
2.	32.31°	2.761	32.35°	2.750	32.39°	2.739
3.	46.08°	1.966	46.09°	1.957	46.13°	1.939
4.	52.28°	1.748	52.42°	1.723	52.62°	1.703
5.	57.65°	1.595	57.79°	1.534	58.11°	1.493
6.	67.80°	1.382	67.93°	1.341	67.99°	1.304

S1. PXRD pattern of MoS$_2$ and BiVO$_4$
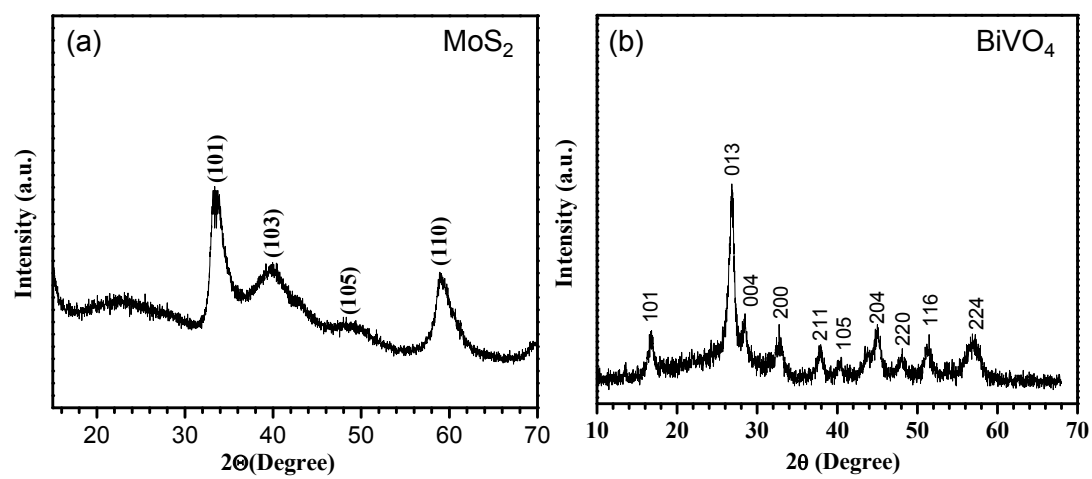
Figure S1. PXRD pattern of bare (a) MoS$_2$ and (b) BiVO$_4$ nanomaterials.
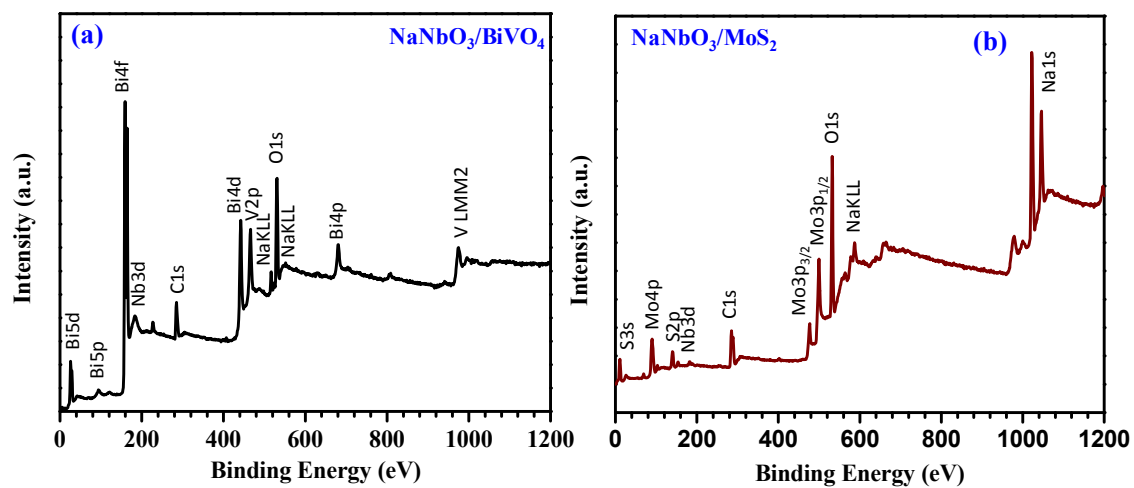
S2. XPS Measurement

Figure S2. XPS measurement of (a) NaNbO$_3$/BiVO$_4$ and (b) NaNbO$_3$/MoS$_2$ heterostructures.

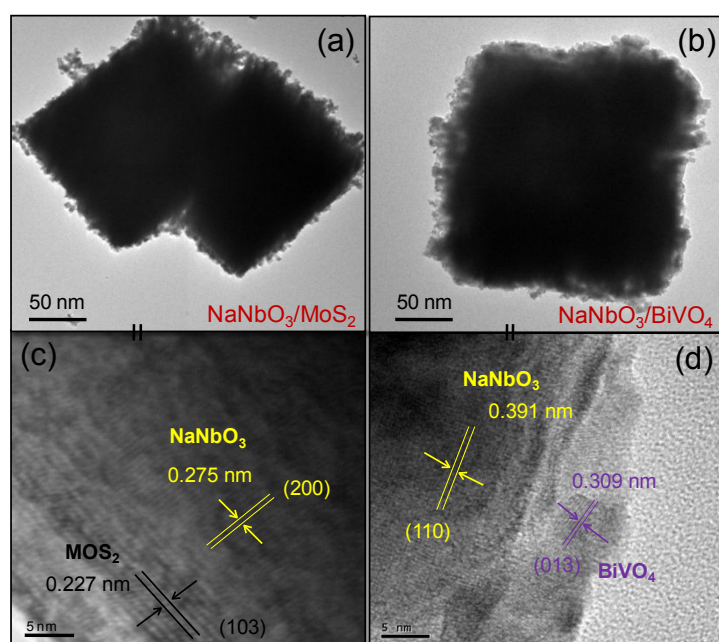**S3. TEM and HRTEM images of core-shell heterostructures**

Figure S3. TEM images of (a) NaNbO$_3$/MoS$_2$ (b) NaNbO$_3$/BiVO$_4$ and HRTEM data of (c) NaNbO$_3$/MoS$_2$ (d) NaNbO$_3$/BiVO$_4$ core/shell heterostructures.
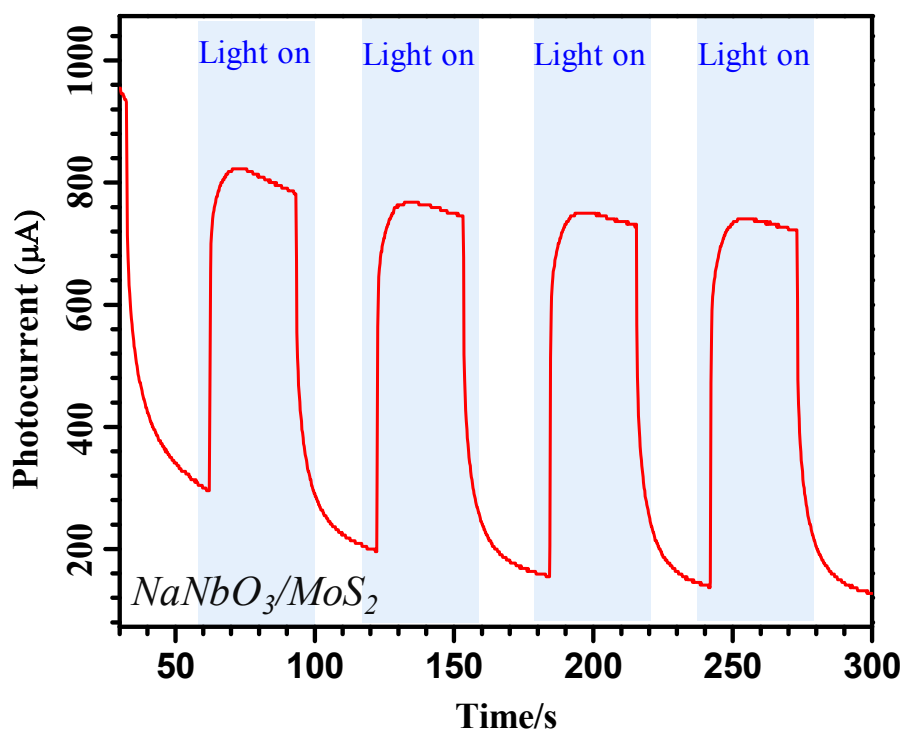
S4. Transient photocurrent responses

Figure S4. Transient photocurrent responses for NaNbO$_3$/MoS$_2$ core–shell heterostructures in 0.5 M Na$_2$SO$_4$ aqueous solution.
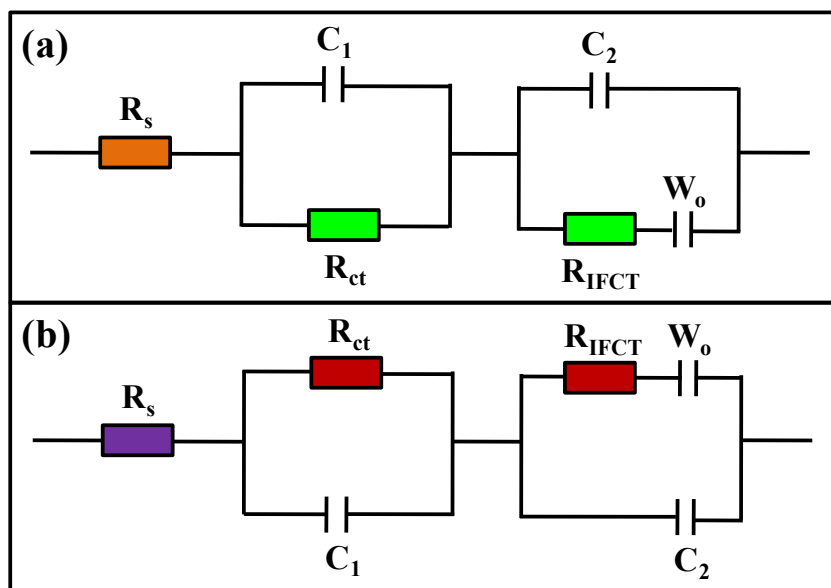
S5. EIS Nyquist plots equivalent circuit

Figure S5. Based on EIS Nyquist plots (a) equivalent circuit of $NaNbO_3/MoS_2$ and (b) $NaNbO_3/BiVO_4$ core–shell heterostructures.

Table S2. Electrochemical impedance spectroscopy Nyquist plot parameters of synthesized core/shell heterostructures.

Samples	R_s/Ω	R_{ct}/Ω	R_{IFCT}/Ω	W/Ω	$C_1/\mu F$	$C_2/\mu F$
$NaNbO_3/MoS_2$	12	8.86	3.4	39.8	70.6	39.3
$NaNbO_3/BiVO_4$	16	12.1	8.36	198.1	64.1	47.9

S6. Photocatalytic degradation activity of BiVO$_4$ and MoS$_2$
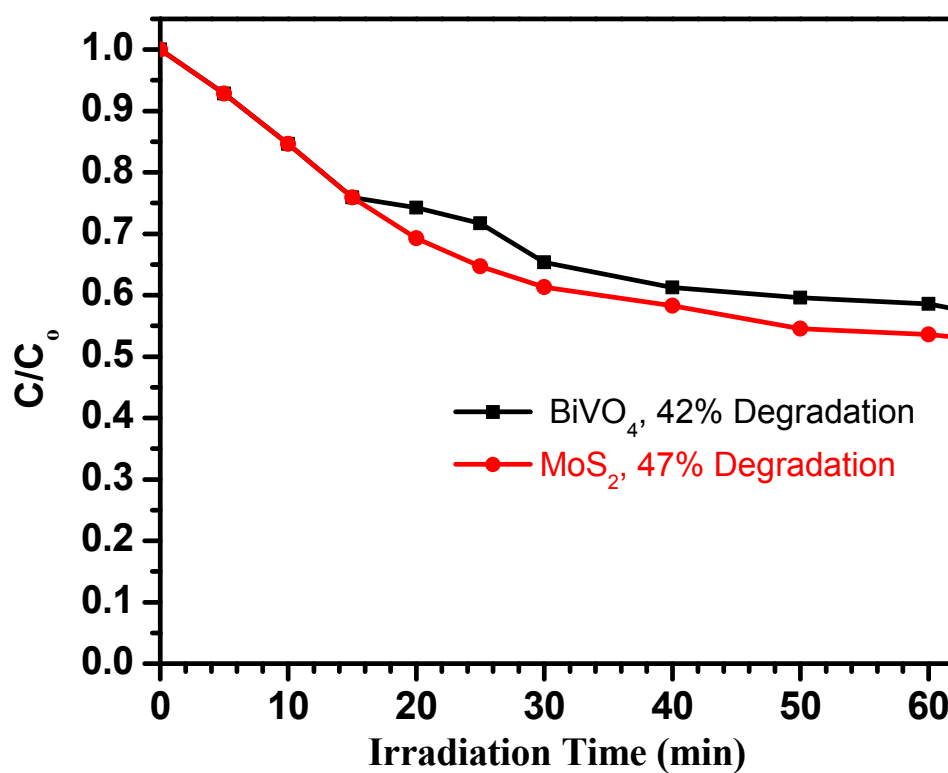

Figure S6. Organic dye Photodegradation by MoS$_2$ and BiVO$_4$ nanomaterials under visible light irradiation.
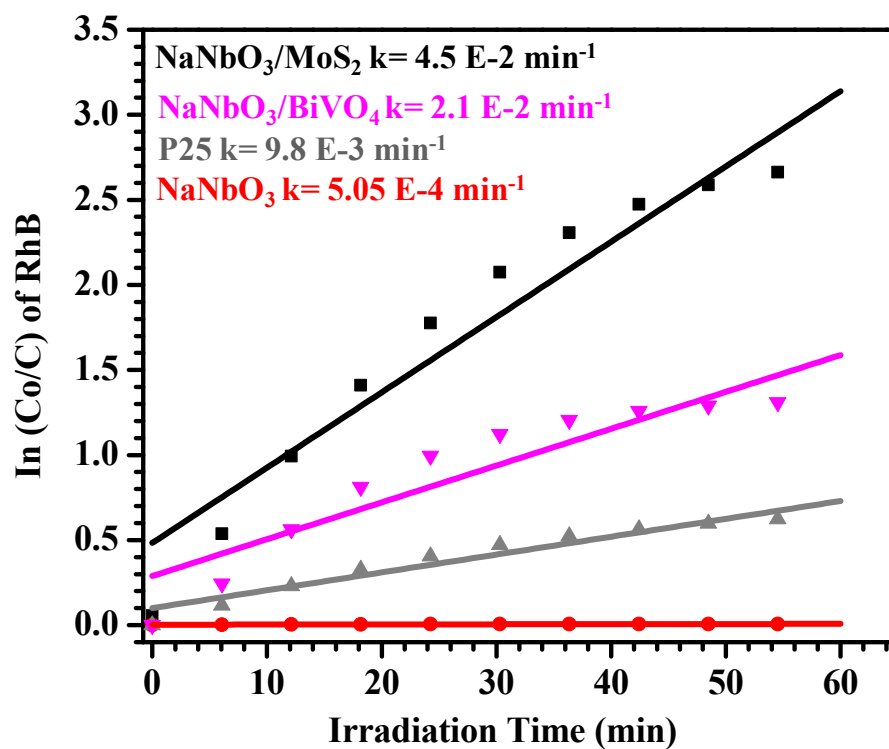
S7. Kinetics plot

Figure S7. Plot of $\ln(C_0/C)$ as a function of visible irradiation time for photocatalysis of RhB solution containing: $NaNbO_3$ nanocubes, Degussa P25, $NaNbO_3/MoS_2$ and $NaNbO_3/BiVO_4$ core/shell heterostructures under visible light irradiation.

Table S3. Band gap and photocatalytic activity of $NaNbO_3$, $P25$-TiO_2, $NaNbO_3/MoS_2$ and $NaNbO_3/BiVO_4$ core-shell heterostructure for degradation of Rh B.

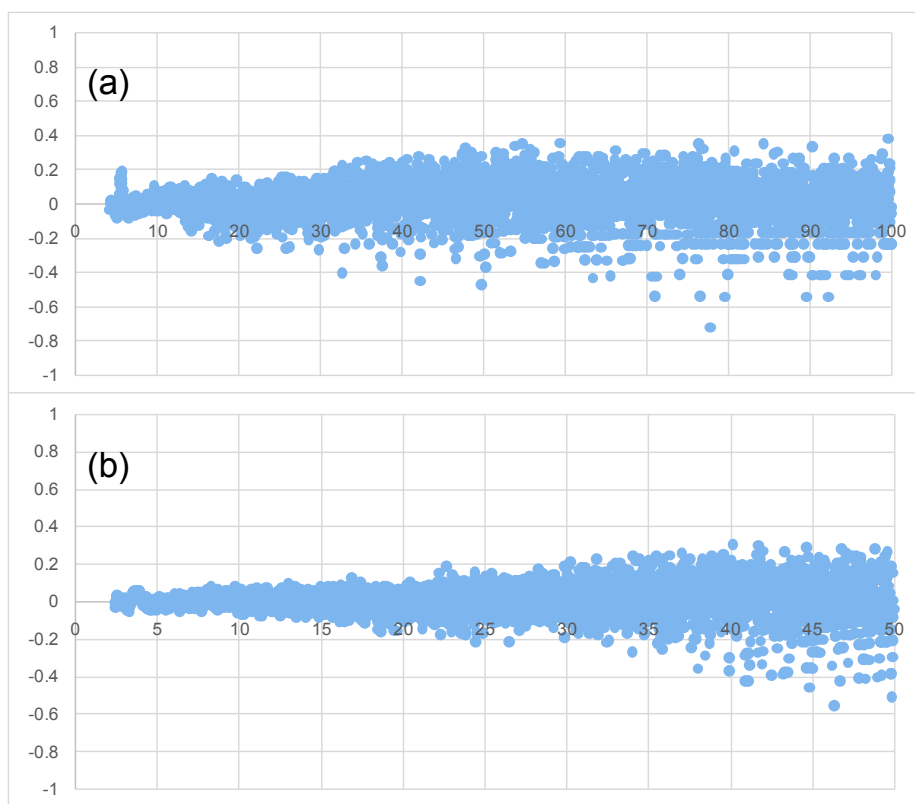| Composition	Band gap (eV)	Degradation Efficiency (%)	Rate constant 'k' (min^{-1})
NaNbO$_3$	3.27	1.1	0.0005
P25	3.1	43.1	0.0098
NaNbO$_3$/MoS$_2$	2.60	95.2	0.045
NaNbO$_3$/BiVO$_4$	2.90	75.6	0.021

S8. Residual fitted function plot

Figure S8. The figure shows the residual plot for the fitted functions to the actual time resolved decay of (a) NaNbO$_3$/BiVO$_4$ and (b) NaNbO$_3$/MoS$_2$ core-shell heterostructures.

References

1. Prabhu, Y. T.; Rao, K. V.; Kumar, V. S. S.; Kumari, B. S. X-Ray Analysis by Williamson-Hall and Size-Strain Plot Methods of ZnO Nanoparticles with Fuel Variation. *World J. Nano Sci. Eng.* **2014**, *4*, 21-28.

2. Monshi, A.; Foroughi, M. R.; Monshi, M. R. Modified Scherrer Equation to Estimate More Accurately Nano-Crystallite Size Using XRD. J. of Nano Sci. Eng. **2012**, *2*, 154-160.

3. Hong, S. J.; Lee, S.; Jang, J. S.; Lee, J. S. Heterojunction BiVO$_4$/WO$_3$ electrodes for enhanced photoactivity of water oxidation *Energy Environ. Sci.*, **2011**, *4*, 1781-1787.

4. Kumar, S. Singh, A. P.; Bera, C.; Thirumal, M.; Mehta, B. R.; Ganguli, A. K. Visible-Light-Driven Photoelectrochemical and Photocatalytic Performance of NaNbO$_3$/Ag$_2$S Core–Shell Heterostructure *ChemSusChem,* **2016**, *9*, 1850-1858.